Role of defects in two-dimensional phase transitions: An STM study of the Sn/Ge(111) system

A. V. Melechko, J. Braun, H. H. Weitering, and E. W. Plummer

Department of Physics and Astronomy, University of Tennessee, Knoxville, Tennessee 37996
and Solid State Division, Oak Ridge National Laboratory, Oak Ridge, Tennessee 37831

The influence of Ge substitutional defects and vacancies on the $(\sqrt{3}\times\sqrt{3})\rightarrow(3\times3)$ charge-density wave phase transition in the α phase of Sn on Ge(111) has been studied using a variable-temperature scanning tunneling microscope. Above 105 K, Ge substitutional defects stabilize regions with (3×3) symmetry that grow with decreasing temperature and can be described by a superposition of exponentially damped waves. At low temperatures, $T\leqslant105$ K defect-defect density-wave-mediated interactions force an alignment of the defects onto a honeycomb sublattice that supports the low-temperature (3×3) phase. This defect-mediated phase transition is completely reversible. The length scales involved in this defect-defect interaction dictate the domain size ($\approx10^4$ Å^2).

I. INTRODUCTION

The concepts of symmetry, dimensionality, and disorder all play a central role in the description of phase transitions.[1] As the dimensionality of a system is reduced, electron correlations play a larger role, and the presence of defects (or broken symmetry) becomes increasingly important. For transitions in highly correlated systems, real-space techniques such as scanning tunneling microscopy (STM) will become the methods of choice in studying the complex phenomena such as phase separation,[2,3] electronic inhomogeneities,[3] and the influence of broken symmetry. Recently, we have reported[4] on the role of Ge substitutional atoms in the $(\sqrt{3}\times\sqrt{3})\rightarrow(3\times3)$ charge-density-wave phase transition[5,6] in the α phase of the Sn on Ge(111). In this system, the Sn forms a very thin metallic film on top of the semiconducting Ge substrate. Theoretical calculations combined with angle-resolved photoemission data indicate that this two-dimensional (2D) system is highly correlated with $U/W >2$ (U is the on-site Coulomb energy and W the bandwidth).[7]

This system and the similar Pb/Ge(111) system have been studied by several groups[4–16] using a multitude of experimental and theoretical techniques. At room temperature, one third of a monolayer (ML) of Sn is arranged to a $(\sqrt{3}\times\sqrt{3})$ structure on Ge(111), with the Sn atoms occupying the T_4 sites of the Ge(111) substrate[10,17] as shown in Fig. 1(a). The unit cell of the α phase is rotated by 30° with respect to the substrate $[(\sqrt{3}\times\sqrt{3}) R30°]$ but is referred to as a $(\sqrt{3}\times\sqrt{3})$ structure throughout this paper. The distance between nearest-neighbor Sn atoms [the $(\sqrt{3}\times\sqrt{3})$ lattice spacing] is 7 Å. When the temperature is lowered, additional diffraction spots appear in the low-energy electron-diffraction (LEED) pattern and indicate a different (3×3) symmetry of the surface. The filled and empty state STM images display (3×3) hexagonal and honeycomb patterns of bright atoms, respectively.[6] This paper explains in detail the measurements reported in an earlier paper[4] and presents different data clarifying the role of the defects in the phase transition.

After a brief experimental Sec. II, the room-temperature $(\sqrt{3}\times\sqrt{3})$ structure will be discussed in Sec. III. The low-temperature ($T\leqslant105$ K) α phase of Sn/Ge(111) is discussed in Sec. IV. Here the crucial role of point defects in aligning (3×3) domains in this phase will be demonstrated. In Sec. V, a comprehensive study of different aspects of the interplay between defects and phase transition will be presented. This section includes a simple superposition model to describe STM images obtained at different temperatures. Section VI presents results regarding the motion of single Ge defects. This paper concludes with a brief discussion of the implications of these measurements. The details associated with the statistical analysis or our STM images are included in the Appendix.

II. EXPERIMENT

The experiments were carried out in a commercial ultra-high vacuum variable-temperature STM. The n-type Ge(111) substrate (Sb doped, 0.18 Ω cm, 5×10 mm^2) was cleaned *in situ* by Ne$^+$ sputtering (1 KeV, 10 min, 20 μA/cm^2) and annealing cycles (15 min at 800 K, measured with an IR pyrometer). Between three and five cycles are required to obtain a well-ordered surface. STM images recorded from the prepared Ge(111) surface at room temperature revealed average terrace widths of about 700 Å.

Sn (purity 99.9999%) was deposited for 5 to 10 min with an evaporation rate of approximately 0.04 ML/min from a commercial Knudsen cell surrounded by a water-cooled shield. The temperature of the Knudsen cell was stabilized at 1000 °C, and the sample was held at room temperature during deposition. After Sn is dosed on the sample, fuzzy (2×2) diffraction spots are visible in the LEED pattern. In order to form the $(\sqrt{3}\times\sqrt{3})$ structure, the sample was annealed at 500 K for approximately 25 min and subsequently cooled to room temperature. Sharp $(\sqrt{3}\times\sqrt{3})$ patterns were obtained after this procedure. $(\sqrt{3}\times\sqrt{3})$-spots were most intense at a beam energy of 43 eV. The sample was then transferred to the STM stage. Close inspection of STM images recorded at room temperature shows that the $(\sqrt{3}\times\sqrt{3})$ phase always coexists with small regions of other Sn submonolayer structures on Ge(111), such as (7×7) and (5×5) reconstructions[17,18] as well as (2×2) patches.[14] The nature of the surface before annealing depended upon the
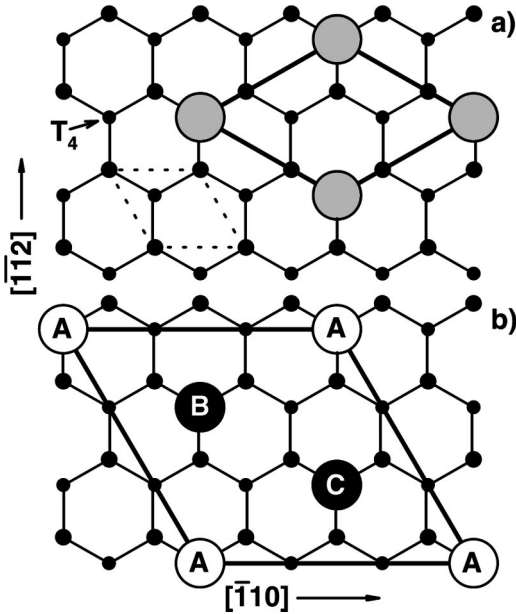
PRB **61**   2235

FIG. 1. Ball model of the two structures of Sn on Ge. (a) $(\sqrt{3}\times\sqrt{3})$ unit cell formed by Sn on Ge(111) at room temperature (α phase). The gray, small black, and tiny black circles correspond to Sn atoms, Ge atoms in the first layer, and second layer, respectively. The Sn atoms occupy T_4 sites of the substrate. (b) (3×3) unit cell of Sn on Ge(111) at $T=50$ K. The large white and black circles correspond to Sn atoms at the corner of and inside the unit cell, respectively. The three different Sn atoms in the unit cell are labeled A, B, and C. In the (3×3) phase, one Sn atom moves up and the other two down.

coverage (deposition time). For low coverage (5 min deposition time), the surface would consist of $(\sqrt{3}\times\sqrt{3})$ and (2×2) reconstructed terraces, while a higher coverage (10 min) produced $(\sqrt{3}\times\sqrt{3})$ areas surrounded by disordered Sn. The $(\sqrt{3}\times\sqrt{3})$ areas seemed to be the same for different coverages. For example, the defect density discussed below does not appear to depend upon the initial coverage. Annealing time and temperature were optimized to give maximum $(\sqrt{3}\times\sqrt{3})$ reconstructed surface. Too high annealing temperature leads to the stable (5×5) and (7×7) reconstructions, and too low of an annealing temperature does not produce a sufficiently ordered surface. On the STM stage, the sample was cooled using a continuous flow cryostat at an average rate of 4 K/min. During the experiments, the temperature T_b of the clamping block of the STM stage was measured and stabilized in the range between 20 K and 300 K with 0.1 K precision. T_b is slightly lower than the actual temperature at the sample, T. T was measured and calibrated to T_b in separate runs both prior to and after the experiments using a chromel-constantan thermocouple attached to the sample. Throughout this paper we refer only to the actual temperature of the sample T, which was reproducible within 5 K.

III. ROOM-TEMPERATURE α PHASE OF Sn

Figure 2(a) is a large area filled state image of the $(\sqrt{3}\times\sqrt{3})$ structure showing several terraces, with an average terrace width of ≈700 Å. The size of the $(\sqrt{3}\times\sqrt{3})$
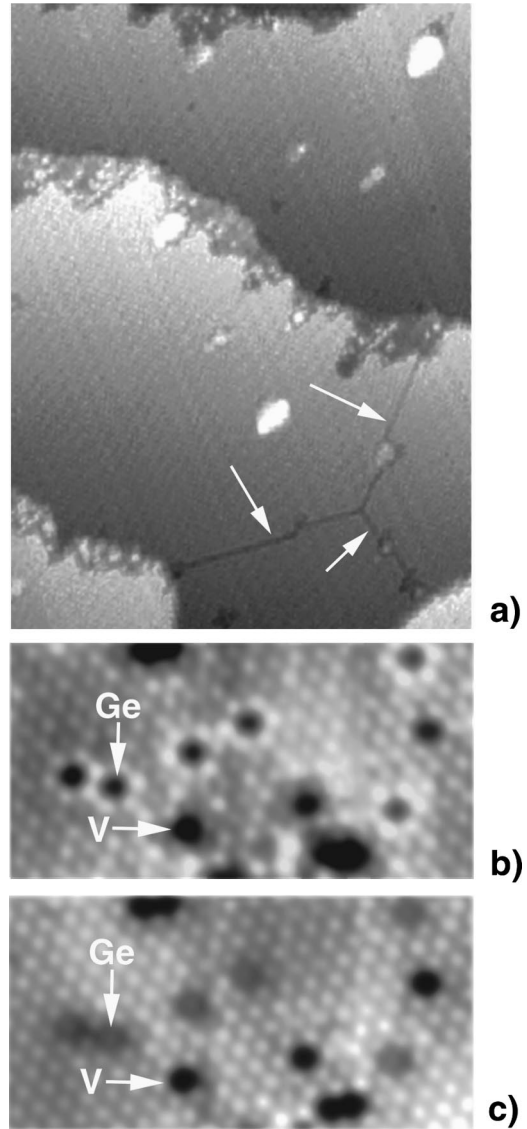

FIG. 2. STM images of the $(\sqrt{3}\times\sqrt{3})$ phase recorded at $T=295$ K. (a) Filled state overview image (600×1000 Å^2, $U_G=-1.3$ V, $I_T=0.1$ nA). Line defects in the $(\sqrt{3}\times\sqrt{3})$ terraces are marked by arrows. (b) Close up filled state image (146×72 Å^2, $U_G=-1.0$ V, $I_T=0.4$ nA). (c) Same as (b) but empty state image ($U_G=+1.0$ V).

domains is dictated by the terrace width and line defects marked by the arrows in Fig. 2(a). The resulting area is on average $\approx5\times10^5$ Å^2. Line defects appear as two atoms wide dark stripes in the filled state image [Fig. 2(a)] but are very narrow in an empty state image. The atomic structure of the $(\sqrt{3}\times\sqrt{3})$ structure has been determined from a LEED (Ref. 8) and surface x-ray-diffraction study.[8,10] The Sn atoms shown in Fig. 1 are located at the T_4 site with a Ge-Sn bond length of 2.87 Å. Within experimental error, all of the Ge-Ge bond lengths are the same as the bulk value of 2.45 Å, but there are considerable bond-angle distortions in both the first and second Ge bilayers.[10]

Several point defects are visible in the filled and empty state images of Figs. 2(b) and 2(c), respectively. About 90% of those defects are substitutional Ge atoms. They will be referred to as Ge defects throughout this paper and appear as black spots surrounded by six bright Sn atoms in filled state
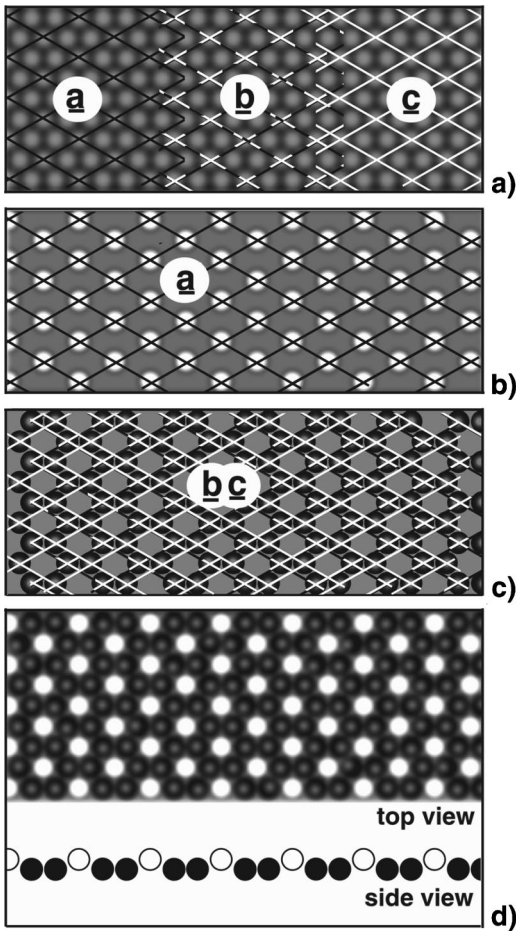
FIG. 3. (a) Three different possibilities to lay (3×3) grids over a $(\sqrt{3}\times\sqrt{3})$ lattice. The $(\sqrt{3}\times\sqrt{3})$ lattice is represented by gray circles. Grids a, b, and c, are illustrated by black, dashed, and white lines, respectively. (b) Hexagonal sublattice of corner atoms of the (3×3) structure coinciding with grid a in (a), called sublattice ''A.'' (c) Honeycomb sublattice formed by sublattices b and c combined. (d) Combination of (b) and (c) results in a lattice that resembles the observed filled state low-temperature STM images. The side view illustrates the vertical rippling of the structure.

images, indicating charge transfer from defects to neighboring atoms.[4,19] Vacancies account for the remaining 10% of defects in α-Sn/Ge(111). They appear as black spots surrounded by six dark nearest-neighbor Sn atoms and six bright second nearest neighbors in the filled state image. Ge defects and vacancies can also be distinguished in the empty state image, where Ge defects appear as gray and vacancies appear as black spots. The identification of Ge substitutional and vacancy defects has been discussed in detail.[20] One Ge defect and one vacancy are labeled in Figs. 2(b) and 2(c). The presence of substitutional atoms from the substrate is a feature common to the α phases of Pb/Ge(111) (Ref. 20) and Sn/Si(111).[21] The average concentration of point defects is $3\pm1\%$ [corresponding to $(6\pm2)\times10^{-4}$ defects/Å^2], consistent with previous reports.[6,22] The defect density did not vary significantly with Sn coverage. An analysis of the STM image in Fig. 3(b) of Ref. 18 [$(\sqrt{3}\times\sqrt{3})$ surface, $\Theta =0.4$ ML] yields a defect density of about 4×10^{-4} defects/Å^2 in agreement with our result. Figure 2(c) presents an empty state STM image of the same region of the

surface as shown in Fig. 2(b). Here Ge defects appear as gray spots surrounded by a ring of Sn atoms that are slightly darker than Sn atoms in perfect $(\sqrt{3}\times\sqrt{3})$ regions. Vacancies are dark in both empty and filled state images because they do not provide any orbital.[20]

IV. LOW-TEMPERATURE PHASE OF α-Sn/Ge(111) AND CORRELATION OF DEFECTS

As the temperature is lowered, the room-temperature $(\sqrt{3}\times\sqrt{3})$ phase gradually converts to an ordered (3×3) phase.[22,23] The details of the temperature dependence of this transition will be discussed in the next section. Here we describe the stable configuration that is seen below 105 K.[4] The filled and empty state STM images of this (3×3) configuration are complementary, with bright protrusions forming a hexagonal and honeycomb pattern, respectively.[6] The structure of this phase has been determined for both Sn (Ref. 10) and Pb (Ref. 11) and is very similar. One of the three Sn atoms in the (3×3) unit cells moves up by ≈0.35 Å while the other two move down by ≈0.02 Å.[10] The vertical rippling of the Sn atoms is accompanied by a small perpendicular (0.17 Å) and parallel (0.12 Å) distortion of the first layer of Ge atoms.[10] In Fig. 1(b), moving atom A up and atoms B and C down can produce this structure. Note that the lattice distortion is localized to the surface region.

The creation of a (3×3) sublattice from the original $(\sqrt{3}\times\sqrt{3})$ lattice is not unique, because three different (3×3) domains exist. It is easy to see how this happens from the structural model shown in Fig. 1(b). There are three Sn atoms in the (3×3) unit cell, which we have been labeled as A, B, and C. If atom A moves up then B and C move down, so that atom A forms a (3×3) hexagonal sublattice as seen in the STM filled state images. But it is equally probable that atom B (C) moves up and atoms A and C $(A$ and $B)$ move down, again forming a (3×3) hexagonal sublattice of B (C) atoms. Figure 3(a) illustrates the three different hexagonal sublattices [black grid (a), dashed grid (b), and white grid (c)], which cover the $(\sqrt{3}\times\sqrt{3})$ lattice (gray balls) completely. Let us assume that the atoms on the sublattice a move up and become bright in the STM image. The observed bright hexagonal sublattice is shown in Fig. 3(b). A combination of the atoms on sublattices b and c form the honeycomb sublattice of dark atoms seen in the filled state image is reproduced in Fig. 3(c). Finally, the combination of the bright hexagonal sublattice formed by sublattice a and the honeycomb sublattice of dark atoms formed from the combination of sublattices b and c is shown in Fig. 3(d), representing the filled state image. Making the atoms in sublattices b and c bright and a dark can reproduce an empty state image. Obviously, we can form three different domains of a hexagonal sublattice by starting with sublattice a, b, or c.

Figure 4(a) is a filled state STM image of the (3×3) phase at 30 K showing the coexistence of two of the three possible domains. The domain on the left is labeled ''A'' (black grid) and the one on the right ''B'' (dashed grid). In the ''A'' domain atoms on sublattice a are bright whereas atoms on sublattices b and c are dark. In domain ''B'' atoms on sublattice b are bright whereas atoms on sublattices a and c are dark. The domain boundary is very abrupt, only a few
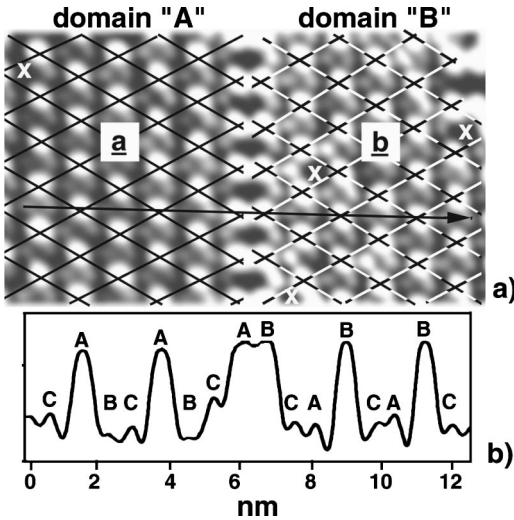
FIG. 4. (a) Filled state STM image (140×42 Å^2, $U_G=-1$ V, $I_T=0.1$ nA) recorded at $T=30$ K. Two different (3×3) domains are marked by different colored grids. Four Ge defects are highlighted by white crosses. A black arrow indicates the position and direction of a line scan shown in (b). (b) Average line scan along the $\langle112\rangle$ direction starting in domain "A."

Å wide. The (3×3) domains have various shapes and sizes but are appreciably smaller than the original ($\sqrt{3}\times\sqrt{3}$) domains. Inspection of many STM images gives an average area for the (3×3) domains of 10^4 Å^2 compared to the average size of the ($\sqrt{3}\times\sqrt{3}$) domains of 5×10^5 Å^2.

The filled state STM image presented in Fig. 5 shows a larger image than Fig. 4, where all three domains labeled "A," "B," and "C" can be seen. White lines highlight the domain boundaries. In general, the domain walls are sharp and parallel to the $\langle112\rangle$ direction except when there are special configurations of defects such as the regions between
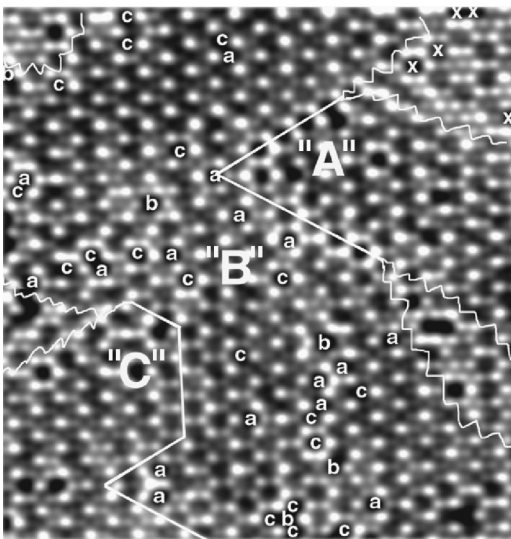

FIG. 5. Filled state image (220×230 Å^2, $U_G=-1$ V, $I_T=0.1$ nA) obtained at $T=50$ K. Three different (3×3) domains are denoted by "A," "B," and "C." White lines highlight domain boundaries. Ge defects are indicated by a, b, and c in domain B according to their lattice position. Outside of domain B Ge defects are indicated by $\times$.

the wiggly white lines. These special regions will be discussed later. The "B" domain is one of the largest we observed with an area of 3.4×10^4 Å^2, containing ≈800 Sn atoms. There are 40 Ge defects in the "B" domain marked by a, b, or c depending upon which sublattice they are located. Amazingly, only five Ge defects are located on the b sublattice where the charge density is maximum. Sixteen defects are on sublattice a and 19 on sublattice c, the preferred sites for Ge defects where the charge density has a minimum.[4,22] Statistically, we find that within each (3×3) domain $\approx90\%$ of the Ge defects are positioned on the charge minimum sites forming a honeycomb sublattice. There is no measurable ordering of the defects within the honeycomb lattice; they populate equally the two equivalent hexagonal sublattices that make up this honeycomb structure. A statistical analysis of the location of the defects at room temperature (165 K, 105 K, and 50 K) was performed and described in the Appendix. At room temperature and at 165 K, Ge defects are randomly distributed on all three sublattices. Upon cooling to 50 K and 105 K, 90% of Ge defects are positioned on the honeycomb sublattice of charge minima within each domain (compare this to 67% for a random distribution).

Finally, we discuss the regions between domains shown in Fig. 5. The presence of Ge defects on charge *maximum* sites has interesting consequences. For example, the straight domain boundary running from about the center of the image in Fig. 5 to its upper-right corner is suddenly interrupted by an inhomogeneous region stabilized by Ge defects positioned in between domain A and B. Here three Ge defects are located on the charge maximum sites of domain A. There are approximately 70 Sn atoms in this region. Fading of the boundary between A and B can also be seen in the middle right part of the image. This region includes four defects, two on sublattice b and two on sublattices a and c, again stabilizing an inhomogeneous structure.

Analysis of the low-temperature STM images of the (3×3) phase have thus produced three surprising observations.

(i) Small (3×3) domains are formed inside of what was a large ($\sqrt{3}\times\sqrt{3}$) domain. On average there are 40 (3×3) domains contained within an original ($\sqrt{3}\times\sqrt{3}$) domain.

(ii) Almost all Ge defects in the low-temperature (3×3) phase are aligned on the charge minimum honeycomb sublattice.

(iii) Small inhomogeneous regions are stabilized by defects in the walls between (3×3) domains.

These observations raise intriguing questions. Why should the large ($\sqrt{3}\times\sqrt{3}$) domains [see Fig. 2(a)] not be converted into one uniform (3×3) domain? Why does the system apparently prefer many energetically costly domain walls (white lines in Fig. 5) over a large (3×3) domain? Observations (ii) and (iii) suggest that Ge defects provide the key for understanding the formation of the structure of the low-temperature phase. The role of defects in the transition from the ($\sqrt{3}\times\sqrt{3}$)$\rightarrow$(3×3) phase will be described in detail in the following section.

V. THE TRANSITION FROM ($\sqrt{3}\times\sqrt{3}$) TO (3×3)

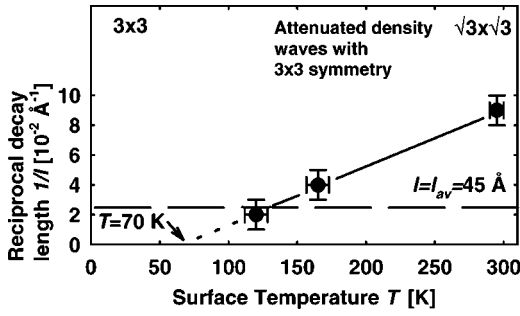STM images become quite complex as the temperature is reduced from room temperature.[4] Damped oscillatory density

FIG. 6. Temperature dependence of the reciprocal decay length $1/l(T)$. The horizontal dashed line corresponds to an average defect-defect distance of 45 Å (Ref. 17). $l(T)$ diverges at $T = 70$ K.

waves, (3×3) in character, are generated by every defect where the extent of the density wave is characterized by a temperature-dependent decay length, $l(T)$. At temperatures between 300 K and 105 K, images are comprised of these interfering density waves, forming complex arrays of bright hexagonal, bright honeycomb, and $(\sqrt{3}\times\sqrt{3})$ coexisting structures. Based on our observations, an *ansatz* for the density waves was proposed,[4]

$$I(\mathbf{r}) = f_{\sqrt{3}\times\sqrt{3}}(\mathbf{r}) + \sum_{n}^{N} A_n e^{-|\mathbf{r}-\mathbf{r}_n|/l(T)}$$

$$\times \sum_{i=1}^{3} \cos[\mathbf{k}_i(\mathbf{r}-\mathbf{r}_n) + \Phi_n]. \qquad (1)$$

$I(r)$ is the brightness of an atom in the filled state image at a position $\mathbf{r}$; $f_{\sqrt{3}\times\sqrt{3}}$ models the $(\sqrt{3}\times\sqrt{3})$ periodicity of the STM images with no defects present. The second term on the right side of Eq. (1) consists of a sum over all attenuated waves induced by N defects with coordinates $\mathbf{r}_n$ and phases Φ_n. It appears sufficient to consider the amplitude A_n as a constant for all defects. Damping is taken into account by introducing the exponential factor with a decay length $l(T)$. Each defect contributes three cosine waves with wave vectors along the three $\langle 112 \rangle$ directions [see Fig. 1(b)]. The outcome of this fitting procedure is reproduced in Fig. 6, showing that the inverse decay length decreases monotonically in the temperature range between 300 K and 120 K.[4] The horizontal line in Fig. 6, labeled $1/l_{av}$, marks the average Ge defect-defect separation of $l_{av} = 45$ Å.

Since defects play such a crucial role in the phase transition, it is appropriate to begin with an analysis of the STM images of defects at room temperature. Figure 7 displays four different filled state images of Ge defects and vacancies recorded at room temperature. In panel (a) a single Ge defect appears as a dark spot.[20,24] The six nearest-neighbor Sn atoms are appreciably brighter than all other Sn atoms in the $(\sqrt{3}\times\sqrt{3})$ structure. The grid on this image shows that a density wave with honeycomb symmetry is created by the Ge defect even at room temperature.[22] Panel (b) shows a single vacancy that creates quite a different density wave. The nearest-neighbor Sn atoms are now dark, and the symmetry of the density wave being set up is similar to the (3×3) hexagonal sublattice. These observations allow for a definitive choice of the phase Φ_n in Eq. (1): $\Phi_n = 0$ for a vacancy and $\Phi_n = \pi$ for a Ge defect.[4] Panel (c) shows a
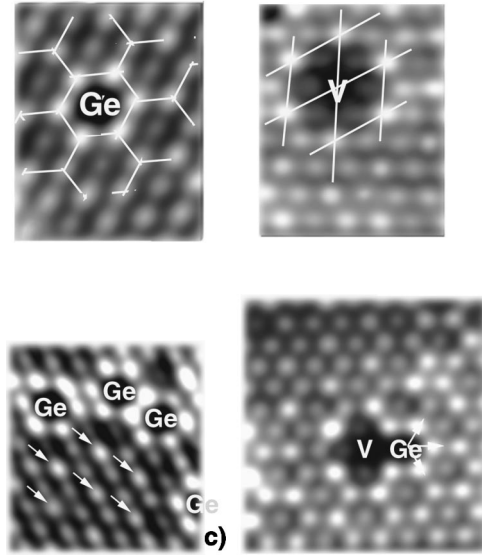

FIG. 7. Filled state STM images ($U_G = -1$ V, $I_T = 0.1$ nA) of defects at room temperature. (a) A single Ge defect with a grid showing the beginning of a honeycomb structure surrounding the defect. (b) A single vacancy defect with the (3×3) hexagonal grid indicated. (c) Four Ge defects. (d) A Ge defect and a vacancy on adjacent sites (65×68 Å^2). The three equivalent $\langle 112 \rangle$ directions of the wave vectors, k_i ($i = 1,3$), in the model, Eq. (1), are marked by white arrows.

region where the Ge defects are close together but on different sublattices. The two Ge defects on the top right are on the same sublattice, which we label a, but the one on the left and the one on the right edge of the image are on the c sublattice. This gives a complex interference pattern of bright and dark atoms that can be seen as far as 3-4 atoms away from the defects. The bright Sn atoms on the lower part of the image resemble a (3×3) hexagonal structure (marked by arrows as a visual aid). Panel (d) shows a vacancy and Ge defect on nearest-neighbor sites. As the temperature decreases, the extent of the defect perturbation grows since $l(T)$ increases [Eq. (1)] and a complicated interference pattern results.

Before showing a comparison of experimental data and simulations from Eq. (1) with 70–100 defects present, it is illustrative to discuss model simulations involving only a few Ge defects. Figure 8 is a set of simulations for different arrays of Ge defects. In panels (a)–(c), the decay length was chosen to be 11 Å, simulating a room-temperature experiment. In panel (a), two Ge defects on different sublattices a and b produce a hexagonal-like pattern on sublattice c. This is a consequence of the superposition of two honeycomb patterns from each Ge defect (Fig. 7). In panel (b), three Ge defects occupy sites on the same sublattice (a). Superposition of waves from these ordered Ge defects yields a honeycomb pattern. Panels (c) and (d) illustrate the influence of the exponential factor in Eq. (1). Here three Ge defects are placed on three different (3×3) sublattices. Ge defects on a and b are closer to each other (bottom) than to the Ge defect at the top (c). When the decay length is only 11 Å [panel (c)], Ge defects produce honeycomb patterns, decaying before they would interfere. If the decay length $l(T)$ is increased to 100 Å (simulating a temperature of ≈ 100 K), a complex pattern is obtained [panel (d)]. Above the Ge defect
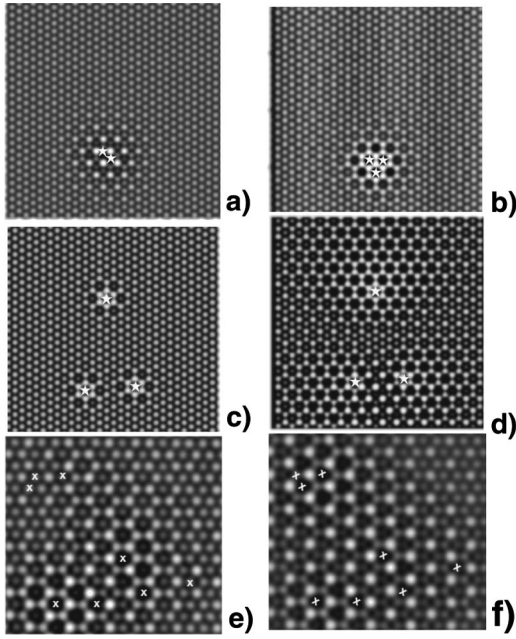
FIG. 8. Simulation for different configurations of Ge defects (labeled by their sublattice position). (a) Two Ge defects on a and b sublattice with $l=11$ Å. (b) Three Ge defects all on a ($l=11$ Å). (c) Three Ge defects on a, b, and c ($l=11$ Å). (d) Same three Ge defects as in panel (c) but $l=100$ Å. (e) Eight defects randomly distributed, a, b, and c ($l=100$ Å). (f) Eight defects aligned on two sublattices a and b ($l=100$ Å).

at the top, the honeycomb pattern expected from a single Ge defect is observed. In between the two Ge defects at the bottom is a hexagonal pattern, while to the right or left of these Ge defects are honeycomb patterns on different sublattices. One important fact is that in between the top and bottom defects a region of $(\sqrt{3}\times\sqrt{3})$ is created as a result of destructive interference. Simulations with eight defects and a decay length of $l=100$ are presented in panels (e) and (f). Defects in panel (e) are randomly distributed on all three sublattices (Fig. 3), three defects on a and b and two on c. The resulting superposition pattern does not resemble a uniform lattice (i.e., it is neither purely honeycomb nor purely hexagonal). In panel (f) we have shifted the two c sublattice defects, one to sublattice a and the other to sublattice b. The superposition yields a nearly perfect hexagonal sublattice with bright atoms occupying sublattice c. Sublattices a and b become dark, [i.e., all defects sit on dark sites (charge-density minima)]. This simulation answers the question of how Ge defects, which on their own generate a honeycomb density wave, can produce a hexagonal pattern at low temperature as seen in Figs. 4 and 5. They align themselves on any two of the three possible sublattices (Fig. 3). The interference pattern from Ge defects randomly distributed on two sublattices, say a and b, produces a hexagonal pattern on the third sublattice c. This is in agreement with images recorded at $T \leq 105$ K, as shown, for example, in Figs. 4 and 5.

Now it is possible to explain how we determined the value of $l(T)$ from experimental data. In principle, it should be quite easy to determine the extent of the density wave from a single Ge defect as a function of temperature. In practice, interference patterns between density waves from nearby Ge defects makes this procedure impossible. Panel
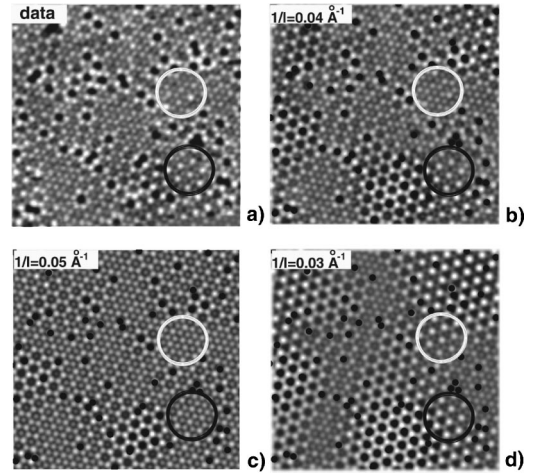

FIG. 9. Comparison of an STM image and simulations for fitting. (a) Filled state STM image (175×180 Å^2, $U_G=-1$ V, $I_T=0.1$ nA), recorded at $T=165$ K. (b) Simulation for $1/l(T)=0.04$ Å^{-1} (best agreement). (c) Simulation for $1/l(T)=0.05$ Å^{-1} (too large). (d) Simulation for $1/l(T)=0.03$ Å^{-1} (too small). The two circles are regions where the interference pattern is very sensitive to the decay length. Inside the white circle the experimental image is $(\sqrt{3}\times\sqrt{3})$ while inside the black circle it is (3×3) hexagonal.

(a) of Fig. 9 shows such a complex interference pattern in a filled state image taken at 165 K. In the simulations, defect sites and type are taken from the experimental image. The best-fit simulation is shown in panel (b), with an inverse decay length $1/l(165$ K$)=0.04$ Å^{-1}. Panels (c) and (d) show the simulations where the inverse decay length is slightly larger, $1/l=0.05$ Å^{-1}, and slightly smaller $1/l=0.03$ Å^{-1}. Our definition of a good fit was that the complex interference patterns between defects seen in the experiment were reproduced in the simulated image. The two circled regions in the experimental image illustrate this procedure. There are no defects inside either the white or black circle, but the effects of defects are quite different. The image inside the white circle is $(\sqrt{3}\times\sqrt{3})$ while a bright hexagonal pattern is created by defects inside of the black circle. The best-fit simulation shown in panel (b) reproduces both of the structures. If the decay length is shortened as it is in panel (c), the $(\sqrt{3}\times\sqrt{3})$ pattern in the white circle is correct, but the image in the black circle is $(\sqrt{3}\times\sqrt{3})$ instead of (3×3) hexagonal as seen in the image. On the other hand, if the decay length is increased too much [panel (d)], a (3×3) hexagonal pattern is created inside the white circle. The decay length used in (b) reproduces the interference patterns in the experimental data, while the decay lengths in (c) and (d) are incorrect. This procedure was used to determine $l(T)$ and the error bars in Fig. 6.

At temperatures between 300 K and 120 K, the surface structure is very complex as reflected in the STM images. Even though a (3×3) LEED pattern appears at 210 K, a true (3×3) phase in STM images only appears below 105 K. At intermediate temperatures, the surface is comprised of an inhomogeneous mixture of hexagonal, honeycomb, and $(\sqrt{3}\times\sqrt{3})$ patches. Even within a region that has a given symmetry, say a (3×3) hexagonal, the intensity of "like" atoms is not uniform. This implies that the structure within
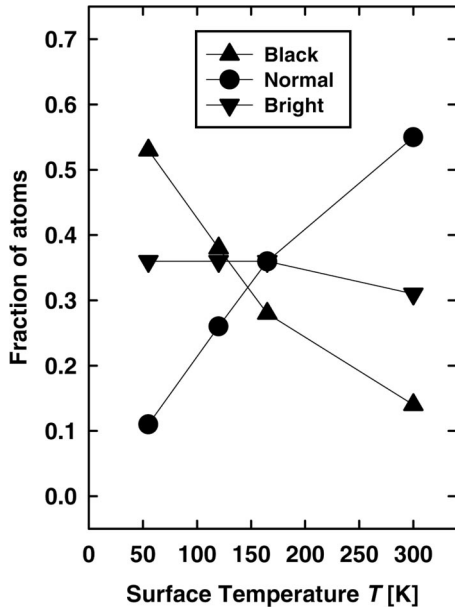
FIG. 10. Fractions of bright, dark, and normal atoms in filled state STM images as a function of temperature. The fractions were determined from averaging over about ten 250×250 Å^2 images for each temperature. ''Normal'' refers to atoms that look like atoms in undistorted regions of filled state images recorded from the room-temperature $(\sqrt{3} \times \sqrt{3})$ phase.

this region is not uniform and not the same as the structure determined at 60 K.[10,11] A simple illustration of the intricacy of this temperature regime can be given by counting the number of bright, dark, and gray atoms in a large set of images as a function of temperature. This procedure is slightly subjective, but inspection of Figs. 2, 5, 7, and 9(a) shows that it is not difficult to classify all atoms into one of the three categories (defects are not counted). Figure 10 is such a plot with data for four different temperatures. The simplest model would have only gray (''normal'') atoms from the $(\sqrt{3} \times \sqrt{3})$ structure at room temperature and a ratio of 33% bright and 67% dark at low temperature from the hexagonal (3×3) structure. As the temperature is decreased from room temperature, the fraction of gray atoms should go to zero and the bright and dark should increase from zero, but always with a 1:2 ratio. Obviously this picture does not reproduce the data in Fig. 10 because we have ignored the Ge defects. At room temperature, there are about $3 \pm 1\%$ Ge defects with six bright atoms surrounding each defect, so we would anticipate $\approx 18 \pm 6\%$ bright atoms. The superposition of waves from defects close together makes some second- and third-nearest neighbors bright and some first-nearest neighbors dark, giving the experimental number of 30% [see Fig. 7(c)]. At low temperature the perfect ratio of one bright for two dark is perturbed by the domain walls as shown in Fig. 5. The branching ratios for bright, dark, and gray at intermediate temperatures is not something that could have been predicted. For example, the fact that the fraction of bright atoms is almost constant is a consequence of the details of the interference patterns. This plot indicates how complicated interpretation of core-level spectra can be without the aid of an STM.[25]

The complex images obtained at intermediate temperature showing both hexagonal and honeycomb structures also ex-
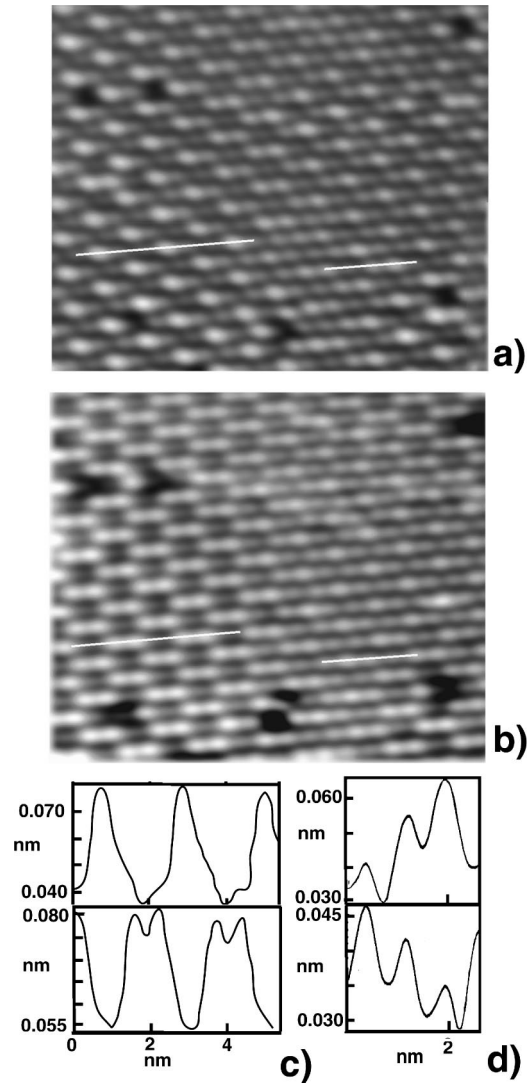

FIG. 11. Complementarity of filled and empty state images $(180 \times 180$ Å^2, $I_T = 0.13$ nA) at $T = 120$ K. (a) Filled state STM image $(U_G = -1$ V). (b) Empty state STM image $(U_G = +1$ V) of the same surface area. A honeycomb pattern is clearly visible in the center portion of this image. The image is fully complementary to (a). (c) Line profiles taken along the lines indicated in the left portion of images (a) and (b). (d) Line profiles taken along the lines marked in the right part of images (a) and (b).

hibit contrast reversal when the bias is changed. This complementarity in the imaging is a key feature of the low-temperature STM image $(T \lesssim 105$ K).[5,6] Figure 11 reveals more details of the bias dependence of (3×3) structures above 70 K. These STM images taken at $T = 120$ K show a region of the surface where both a hexagonal and honeycomblike structure exist. The filled state image is shown in (a) and the empty state image in (b). The bright atoms in the empty state image are dark in the filled state image and vice versa. We obtain complementary filled and empty state images at all temperatures. The line scan in Fig. 11(c) taken at the left part of the images demonstrates that we have two dark and one bright atom in the (3×3) unit cell in the filled state image (hexagonal) and two bright and one dark in the empty state image (honeycomb). This is the behavior for the low temperature (3×3) first reported at $T \lesssim 60$ K by

Carpinelli *et al.*[5] The structure of this configuration is one Sn atom up and two Sn atoms down in a (3×3) cell. The right part of the images in Fig. 11, however, includes an example in which all three atoms of a unit cell appear different. This is corroborated by line scans presented in Fig. 11(d), showing that the two images are still complementary. It is reasonable to assume that differences in brightness of the atoms are associated with rearrangement of charge accompanied by a vertical distortion of the Sn atoms. If this assumption is correct, then there are regions of this image (center portion) where the (3×3) structure consists of two atoms up and one atom down. We have obtained many STM images similar to Fig. 11 for temperatures ranging from 120 K to 200 K. Surfaces such as shown in Fig. 11 undoubtedly give rise to strong diffraction spots with (3×3) symmetry. However, different regions of the surface will contribute different diffraction intensities due to the variations in the arrangement of atoms within (3×3) cells, rendering the determination of unit-cell structures ambiguous.

VI. MOTION AND CORRELATION OF DEFECTS AT LOW TEMPERATURE

Ge defects rule the nature of the $(\sqrt{3}\times\sqrt{3})\rightarrow(3\times3)$ phase transition in this system. They pin damped density wave distortions at temperatures below room temperature, interact with these waves, and align themselves onto the favorable charge minimum honeycomb sublattice at low temperature. One remaining question to be answered is at what temperature they move. Two arguments can be presented that lead to different pictures of this process. The first picture is based on the premise that the divergence of the decay length $l(T)$ is the critical parameter. In this model, *independent of the defect concentration*, there is a phase transition at ≈70 K that forces some of the Ge defects to move into favorable lattice sites on the honeycomb sublattice. The second picture is based upon the density of defects and the defect-defect density-wave-mediated interactions. In this picture, the phase transition happens when the interaction energy between the defects exceeds the activation energy to move the Ge defects. This length scale is represented by l_{av} shown in Fig. 6 and is approximately equal to 40 Å for this system. At a temperature where $l(T)\approx l_{av}$, the complex density waves mediate a defect-defect interaction.

To answer the question about the temperature at which Ge defects are aligned, a statistical analysis of STM images at various temperatures was performed. The procedure and the definition of the correlation probability P_C are given in the Appendix, and the results are plotted in Fig. 12. The filled circles in Fig. 12 represent the results of the analysis of the data recorded during a cooling cycle. The sample was prepared, the $(\sqrt{3}\times\sqrt{3})$ confirmed, and then the sample was cooled to the temperature T. The STM images were randomly sampled with a sampling area (SA), which was taken slightly smaller (80×80 Å^2) than the average size of the (3×3) domains at low temperature. The number of Ge defects on all three sublattices was recorded. $P_C\equiv0\%$ if the Ge defects equally populated all three sublattices (a, b, and c); $P_C\equiv100\%$ if all defects are distributed only on two sublattices, equally populating each of them. Because of the finite size of the images and existence of domain boundaries at low
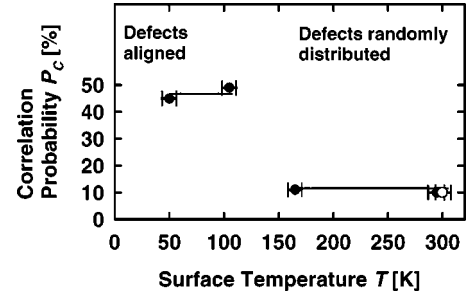

FIG. 12. Temperature dependence of the correlation probability P_c (see text). Data points marked by filled circles were determined using the analysis described in the Appendix after cooling the sample to temperature T. The open circle at $T=300$ K corresponds to an experiment where the sample was cooled to $T=30$ K and subsequently warmed up to room temperature.

temperature, a statistical analysis of well-defined computer generated distributions was performed to facilitate the interpretation of experimental data. A statistical analysis of a computer generated random distribution of Ge defects on all three sublattices a, b, and c gives $P_C=10\%$, compared to $P_C\approx50\%$ for computer generated distributions where the area was divided into sections (''domains'') with defects perfectly aligned on the honeycomb sublattice in that section (i.e., the defects are placed only on a and b inside section 1, and only on c and b in section 2, and so on). The correlation probability for the ''aligned'' distribution is $P_C\approx50\%$, P_C is not 100% because the SA straddles the ''domain'' boundaries in the random sampling procedure. The result of the statistical analysis of experimental STM images obtained at different temperatures is shown in Fig. 12. It shows that the defects are randomly distributed for temperatures $T>150$ K. In stark contrast, the correlation probability is $\approx50\%$ for images taken at 50 K and 105 K. Evidently, Ge defects align themselves at 105 K, a temperature above the projected transition temperature of 70 K based on a diverging decay length. Sufficient data have not been recorded at 120 K to perform the statistical analysis, but the absence of domain walls at this temperature implies that the Ge defects have not aligned. Therefore, the transition temperature for this defect density is somewhere between 105 K and 120 K.

The following experiment was conducted to investigate the reversibility of the $(\sqrt{3}\times\sqrt{3})\rightarrow(3\times3)$ phase transition. After preparing a good $(\sqrt{3}\times\sqrt{3})$ structure, the sample was cooled to 40 K and held there for two hours producing the (3×3) domain structure described in Sec. IV. Subsequently, the sample was warmed up to room temperature, and a statistical analysis of the Ge-defect distribution was performed. Defects were distributed randomly on all three sublattices (open circle data point in Fig. 12). *The phase transition is completely reversible.*

Our picture implies a long-range density-wave-mediated interaction between defects. The consequence of this interaction has been directly observed in several STM images. Figure 13 shows two empty state STM images of the same area taken at $T\approx120$ K,[26] illustrating the effects caused by a change in the defect distribution. In panel (a) of Fig. 13 two different (3×3) regions are marked by black and white grids (sublattices). Since these are empty state images, the low-temperature (3×3) structure is now represented by a bright
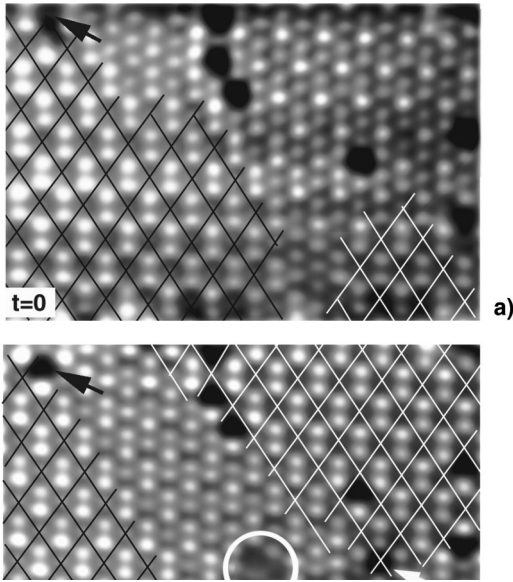
FIG. 13. Empty state STM images at $T = 100$ K (140×90 Å^2, $U_G = 1$ V, $I_T = 0.1$ nA) recorded 1 min apart. Two different (3×3) regions (honeycomb pattern) are marked by black and white grids. (a) The black arrow indicates a Ge defect. (b) A *new* vacancy (see text) is labeled by a white arrow. Note the dramatic change in the (3×3) regions as a response to the appearance of the vacancy. The white circle marks the Sn atom, which has been removed from its original site. The Ge defect labeled by a black arrow has moved downwards by one lattice spacing.

honeycomb sublattice. The image in panel (b) is from the same area, taken one minute later. Comparison of these images reveals a dramatic change in surface morphology associated with the appearance of a vacancy in Fig. 13(b) (denoted by a white arrow). As a consequence, another (3×3) reconstructed region shows up in the upper right part of Fig. 13(b) (white grid) while the other (3×3) region (black grid) is apparently pushed away from the vacancy. The circled protrusion is interpreted as the image of the Sn atom, which was kicked out when the vacancy was formed. It has moved about 35 Å. Also the motion of a single Ge defect to an adjacent site can be seen in the upper left-hand corner (black arrow) of both panels. It is difficult to determine what created the vacancy, either thermal fluctuations or the tip, but these observations illustrate the effective long-range interaction between the density waves and the defects. Notice also that Fig. 13(a) again shows the coexistence of honeycomb, hexagonal, and $(\sqrt{3} \times \sqrt{3})$ patches.

In summary we find that defect-defect density-wave-mediated interactions drive the phase transition to the (3×3) low-temperature structure. When a single defect moves under the influence of this force, it causes a domino effect, moving (aligning) other defects. The length scale of the defect-defect density-wave-mediated interaction dictates the domain size.

VII. CONCLUSION

The results presented in the paper show conclusively that the defect-defect density-wave-mediated interaction drives the $(\sqrt{3} \times \sqrt{3}) \rightarrow (3 \times 3)$ phase transition in α-Sn/Ge(111) system. When the temperature-dependent decay length $l(T)$

becomes comparable to the average defect-defect spacing $l_{av} = 45$ Å, Ge defects start to interact and realign onto the honeycomb sublattice.

The realignment of Ge defects locks in the (3×3) phase; $l_{av} = 45$ Å dictates the domain size induced by density wave pattern. With the Ge-defect density present on this surface, the transition temperature is 105 K $\leqslant T_c \leqslant 120$ K. This observation raises many interesting speculations and questions.

(i) What are the kinetics and energetics associated with defect motion and domain-wall formation?

(ii) What would happen if we could create a surface with only one Ge defect inside of a $(\sqrt{3} \times \sqrt{3})$ domain? There would be a transition to a honeycomb (3×3) sublattice (filled state image) at 70 K (Fig. 6). This (3×3) structure would be two Sn atoms up and one down. Likewise, if we could create only one vacancy in a $(\sqrt{3} \times \sqrt{3})$ domain, there would be a transition to a hexagonal (3×3) structure at 70 K. This (3×3) structure would be one Sn atom up and two down.

(iii) Would there be a phase transition from $(\sqrt{3} \times \sqrt{3})$ $\rightarrow (3 \times 3)$ if the surface were defect free? If so, would the stable structure be hexagonal or honeycomb?

(iv) The data and interpretations suggest that if the defect density could be controlled then both the transition temperature 105 K $\leqslant T_c \leqslant 120$ K and domain sizes could be tuned. If the defect density is decreased the transition temperature would decrease and the domain size increase.

APPENDIX: STATISTICAL ANALYSIS OF STM IMAGES

Our method of counting defects is illustrated in Fig. 14. Figure 14(a) shows a ball model of the $(\sqrt{3} \times \sqrt{3})$ lattice. The white circles correspond to Sn atoms. About 10% of the Sn atoms are substituted by point defects (black circles). This model resembles typical STM images that were recorded at room temperature. A unit consisting of $12 \times 12 = 144$ atoms, which will be referred to as sampling area (SA), is highlighted in Fig. 14(a). This particular SA contains seven defects. From each STM image of a series of 15 images ($N_I = 15$) recorded at a temperature T, 25 SA's ($N_S = 25$) were *randomly* selected and analyzed. The size of an SA (length of an edge: ≈ 80 Å) is slightly smaller than the typical size of a (3×3) domain at low temperatures (diameter: $d_{3 \times 3} \approx 100$ Å).

The steps of the analysis are demonstrated in Figs. 14(b)–14(d). In Fig. 14(b), a hexagonal grid a (cf. Sec. IV) is laid over the SA. Only one of seven defects [marked by an arrow in Fig. 14(b)] coincides with sublattice a. The two other possibilities to overlay a (3×3) grid on a $(\sqrt{3} \times \sqrt{3})$ lattice, grids b and c, are illustrated in Figs. 14(c) and 14(d), respec-
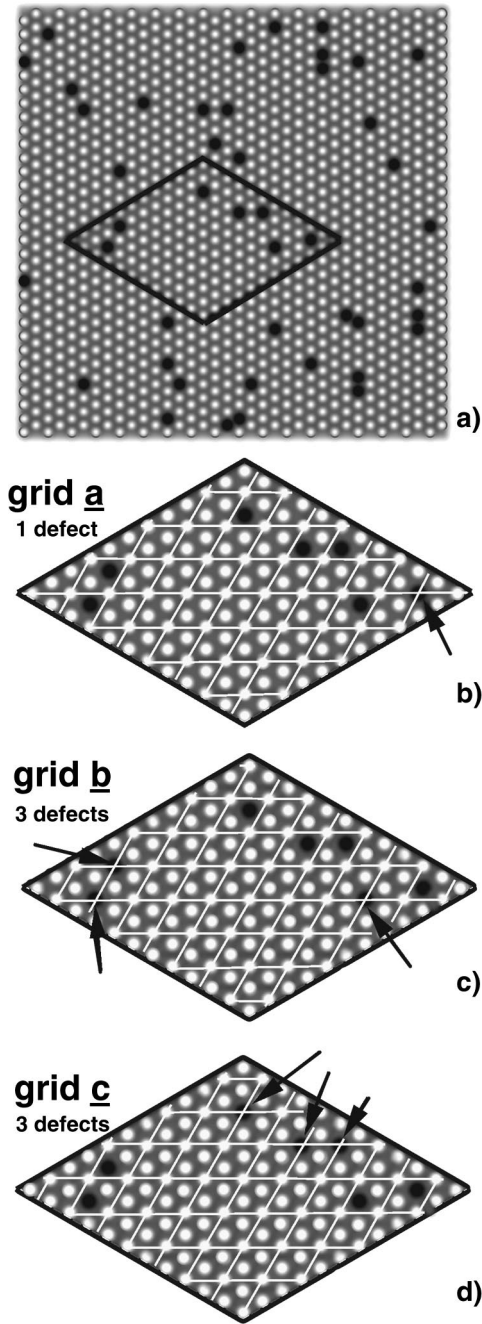
FIG. 14. (a) Ball model of a $(\sqrt{3} \times \sqrt{3})$ surface with randomly distributed Ge defects. Open and black circles represent Sn atoms and Ge defects, respectively. A sampling area consisting of 12×12 atoms is highlighted (see text). (b)–(d) Enlarged drawing of the sampling area shown in (a). Three different possibilities to overlay a (3×3) grid on a $(\sqrt{3} \times \sqrt{3})$ structure (grids a, b, and c) are shown. Black arrows indicate defects that coincide with the (3×3) grid.

tively. In either case, three defects (again marked by arrows) coincide with grids b and c, respectively. According to our observations presented in Sec. IV, the system prefers (3×3) domains with minimal amounts of Ge defects on charge maxima sites. Therefore, it is reasonable to assume that a (3×3) domain ''A'' (cf. Sec. IV) is formed in the SA of Fig. 14 because only one of seven defects [Fig. 14(a)] would coincide with a charge-density maximum.
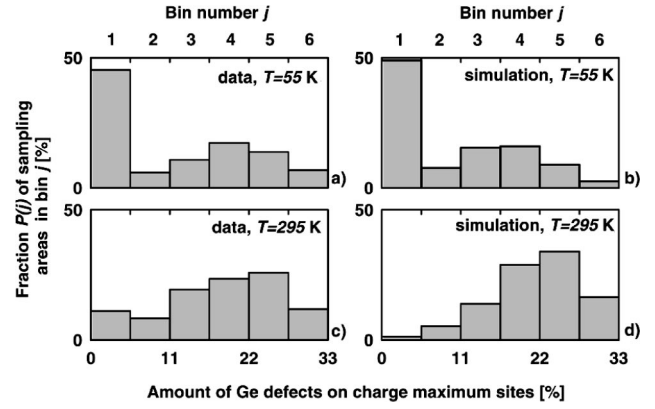

FIG. 15. Probability of finding a certain amount of defects on (3×3) charge maximum sites deduced from a statistical analysis of STM images (see text). (a) Results for STM images recorded at $T = 55$ K (LT). (b) Distribution for a computer generated defect distribution which takes the existence of domain boundaries in the (3×3) phase into account. (c) Analysis of STM images recorded at $T = 295$ K (RT). (d) Results for computer generated images with a random defect distribution.

Thus, the fraction n_{il} of defects that would occupy charge maxima site of the ith SA taken from the lth image is

$$n_{il} = \frac{\min(N_a^{il}, N_b^{il}, N_c^{il})}{N_a^{il} + N_b^{il} + N_c^{il}}, \quad i = 1, \ldots, N_S, \quad l = 1, \ldots, N_I,$$

(A1)

where N_a^{il}, N_b^{il}, N_c^{il}, are the numbers of defects coinciding with sublattices a, b, and c, respectively. For the SA shown in Fig. 14, we obtain $N_a^{il} = 1$, $N_b^{il} = N_c^{il} = 3$, and $n_{il} = 1/7 \approx 0.14$. It follows immediately from Eq. (A1) that $0 \leq n_{il} \leq 0.\overline{33}$ for all i and l. The fractions n_{il} were calculated for each SA. Then, each SA was counted in one out of six bins labeled j, $j = 1, \ldots, 6$. Each bin represents a range of the width $0.\overline{33}/6 \approx 0.055$ of n_{il} values, i.e., the bin $j = 1$ covers all SA's with $0 \leq n_{il} < 0.055$, bin $j = 2$ covers all SA's with $0.055 \leq n_{il} < 0.11$, and so on. The SA shown in Fig. 14 ($n_{il} \approx 0.14$) contributes to bin $j = 3$. Generally, the contribution p_j^{il} of the ith SA selected from image l to bin j can be written in the form

$$p_j^{il} = \begin{cases} 1 & \text{if } \dfrac{j-1}{6} \leq 3n_{il} < \dfrac{j}{6} \\ 0 & \text{otherwise}, \end{cases} \quad j = 1, \ldots, 6. \quad (A2)$$

Finally, the fraction $P(j)$ of SA's in bin j is determined by summarizing over all p_j^{il},

$$P(j) = \frac{1}{N_I N_S} \sum_{i,l} p_j^{il}. \quad (A3)$$

Note that $\Sigma_j P(j) = 1$. The case $j = 1$ deserves particular attention since in SA's that contribute to bin $j = 1$, the number of defects on one sublattice, is practically zero (i.e., the defects occupy two out of three sublattices). This corresponds to the alignment of defects found in (3×3) domains at $T \leq 100$ K (Sec. IV). Therefore, $P(j=1)$ is called *correlation probability* P_c, $P_c = P(1)$ (cf. Fig. 12).

The results of the analysis of STM images recorded at $T = 295$ K and $T = 55$ K, as well as computer-simulated images are compiled in Fig. 15. Computer-simulated images of different defect distributions (e.g., random on all three sublattices a, b, and c, or random on only two sublattices) were generated and analyzed to assist with the interpretation of the distributions $P(j)$ determined from experimental STM images.

About 50% of the selected SA's from STM images at $T = 55$ K contribute to bin $j = 1$ as illustrated in Fig. 15(a). This is in agreement with the observation that Ge defects in images recorded at $T = 55$ K are located on the honeycomb sublattice formed by two out of three (3×3) sublattices. The small but not negligible fractions of SA's in bins $j > 1$ in Fig. 15(a) are due to situations where the SA lies in two (3×3) domains, for example, types A and B. Such cases are not unlikely as the size of the SA is only slightly smaller than the average domain diameter. To confirm these conclusions, a statistical analysis [Eqs. (A1)–(A3)] of 15 *computer-simulated* low-temperature images was carried out. The simulated images were constructed from a $(\sqrt{3} \times \sqrt{3})$ lattice similar to the one shown in Fig. 14(a). Each lattice was randomly divided in three or four domains. Each domain resembled a perfect (3×3) domain A, B, or C, as defects were randomly distributed only on two randomly chosen sublattices. The results of the analysis of simulated images are presented in Fig. 15(b) and are in good agreement with the results in Fig. 15(a). The analysis yields $P(j = 1) = 1$ and $P(j > 1) = 0$, if the existence of several domains in each simulated image is ignored and all defects are randomly distributed on only two sublattices (e.g., a and b).

A significantly different distribution $P(j)$ is obtained if STM images are recorded at $T = 295$ K. These are analyzed following the procedure described above. Figure 15(c) illustrates that in this case only 10% of the SA's belong to bin $j = 1$. To prove that Fig. 15(c) indeed reflects a *random* distribution of defects, 15 computer-simulated images with random defect distribution [cf. Fig. 14(a)] were analyzed. The results are shown in Fig. 15(d) and in fair agreement with Fig. 15(c). Hence, our statistical analysis clearly proves that Ge defects are randomly distributed at room temperature.

[1] L. D. Landau and E. M. Lifshitz, *Statistical Physics* (Pergamon Press, Oxford, 1980), Pt. 1, p. 459.

[2] A. Moreo, S. Yunoki, and E. Dagotto, Science **283**, 2034 (1999).

[3] S. A. Kivelson, E. Fradkin, and V. J. Emery, Nature (London) **393**, 550 (1999).

[4] A. V. Melechko, J. Braun, H. H. Weitering, and E. W. Plummer, Phys. Rev. Lett. **83**, 999 (1999).

[5] J. M. Carpinelli, H. H. Weitering, E. W. Plummer, and R. Stumpf, Nature (London) **381**, 398 (1996).

[6] J. M. Carpinelli, H. H. Weitering, M. Bartkowiak, R. Stumpf, and E. W. Plummer, Phys. Rev. Lett. **79**, 2859 (1997).

[7] F. Flores, J. Ortega, and R. Perez, Surf. Rev. Lett. **6**, 411 (1999).

[8] J. S. Pedersen, R. Feidenhans'l, M. Nielsen, K. Kjaer, F. Grey, and R. L. Johnson, Surf. Sci. **189/190**, 1047 (1987).

[9] A. Goldoni and S. Modesti, Phys. Rev. Lett. **79**, 3266 (1997).

[10] J. Zhang, Ismail, P. J. Rous, A. P. Baddorf, and E. W. Plummer, Phys. Rev. B **60**, 2860 (1999)

[11] A. Mascaraque, J. Avila, J. Alvarez, M. C. Asensio, S. Ferrer, and E. G. Michel, Phys. Rev. Lett. **82**, 2524 (1999).

[12] J. Avila, A. Masacarque, E. G. Michel, M. C. Asensio, G. LeLay, J. Ortega, R. Perez, and F. Flores, Phys. Rev. Lett. **82**, 442 (1999).

[13] R. I. G. Uhrberg and T. Balasubramanian, Phys. Rev. Lett. **81**, 2108 (1998).

[14] G. Le Lay, V. Y. Aristov, O. Boström, J. M. Layet, M. C. Asensio, J. Avila, Y. Huttel, and A. Cricenti, Appl. Surf. Sci. **123/124**, 440 (1998).

[15] S. Scandolo, F. Anciletto, C. L. Chairotti, G. Santoro, S. Serra, and E. Tosatti, Surf. Sci. **402-404**, 808 (1998); G. Santoro, S. Scandolo, and E. Tosatti, Phys. Rev. B **59**, 1891 (1999).

[16] J. P. Rodriguez and E. Artacho, Phys. Rev. B **59**, R705 (1999).

[17] M. Göthelid, M. Hammar, C. Törnevik, U. O. Karlsson, N. G. Nilsson, and S. A. Flodström, Surf. Sci. **271**, L357 (1992).

[18] M. Göthelid, M. Björkqvist, T. Grehk, G. Le Lay, and U. O. Karlson, Phys. Rev. B **52**, R14 352 (1995).

[19] R. Stumpf, J. M. Carpinelli, and H. H. Weitering, Phys. Rev. B **59**, 15 779 (1999).

[20] J. M. Carpinelli, H. H. Weitering, and E. W. Plummer, Surf. Sci. **401**, L457 (1998).

[21] C. Törnevik, M. Göthelid, M. Hammar, U. O. Karlsson, N. G. Nilsson, S. A. Flödström, C. Wigren, and M. Östling, Surf. Sci. **314**, 179 (1994).

[22] H. H. Weitering, J. M. Carpinelli, A. V. Melechko, J. Zhang, M. Bartkowiak, and. E. W. Plummer, Science **285**, 2107 (1999).

[23] J. M. Carpinelli, Ph.D. thesis, University of Pennsylvania, 1997 (unpublished).

[24] L. Seehofer, G. Falkenberg, and R. L. Johnson, Surf. Sci. **290**, 15 (1993).

[25] T. E. Kidd, T. Miller, and T.-C. Chiang, Phys. Rev. Lett. **83**, 2789 (1999).

[26] These images were taken on a different instrument where the temperature was not calibrated. The temperature has been determined using our fitting procedure of simulated STM images [Eq. (1)] to determine $l(T)$ and Fig. 6. Due to the small area imaged, there is an appreciable error in determination of the temperature ($\Delta T = \pm 20$ K), which is estimated to be 120 K. Because sharp domain boundaries were absent in this image, it is certainly above the phase-transition temperature and above 105 K.